

## Factors affecting pre-failure instability of sand under plane-strain conditions

D. WANATOWSKI\* and J. CHU†

Experimental data obtained from a plane-strain apparatus are presented in this paper to show that a pre-failure instability in the form of a rapid and sustained increase in strain rate can occur for both contractive and dilative sand under fully drained conditions. However, this type of instability is different from the runaway type of instability observed under undrained conditions, and has therefore been called conditional instability. Despite the differences, the conditions for both types of instability are the same for contractive sand. There are also other factors that affect the pre-failure instability of sand observed in the laboratory. These include the stress ratio, void ratio, sand state, load control mode and reduction rate of the effective confining stress. In this paper, these factors are discussed and analysed using experimental data obtained from undrained instability (or creep) tests and constant shear drained (CSD) tests carried out under plane-strain conditions.

**KEYWORDS:** failure; laboratory tests; liquefaction; pore pressures; sands; slopes

Cette communication présente des données expérimentales obtenues avec un appareil à déformation plane dans le but de démontrer qu'une instabilité pré-rupture, sous forme d'une augmentation rapide et soutenue de la vitesse de déformation, peut se produire pour des sables en contractif et dilatif, en présence d'un drainage intégral. Toutefois, ce type d'instabilité se distingue du type d'instabilité galopante relevée en présence de conditions non drainées, et a été dénommé, pour cette raison, instabilité conditionnelle. En dépit des différences, les conditions propres à ces deux types d'instabilité sont les mêmes pour le sable contractif. D'autres facteurs également affectent l'instabilité pré-rupture du sable, observée en laboratoire. Parmi ceux-ci, indiquons le rapport des contraintes, l'état du sable, le mode de contrôle de la charge, et le taux de réduction des contraintes de confinement efficaces. Dans la présente communication, on discute et on analyse ces facteurs sur la base de données expérimentales obtenues avec des essais d'instabilité non drainée (ou de fluage) et des essais de cisaillement constant drainés (CSD), effectués en présence de déformations planes.

### INTRODUCTION

Failure of a granular soil slope is often associated with liquefaction or instability of sand. In the laboratory, liquefaction and instability behaviours of sand have been observed mainly for loose sand under undrained conditions (Casagrande, 1975; Lade, 1993; Leong *et al.*, 2000). Based on these observations, instability or static liquefaction occurring for loose sand under undrained conditions has been considered as the main factor causing the failure of loose granular soil slopes. However, there are cases where instability has occurred under essentially drained conditions. For example, in the re-analysis of the Wachusett Dam failure in 1907, Olson *et al.* (2000) concluded that the failure was triggered mainly by static liquefaction that occurred under completely drained conditions. Through laboratory model tests, Eckersley (1990) observed that the pore water pressure increase in the gentle granular soil slope was a result, rather than the cause, of flow slide. In other words, static liquefaction had occurred for loose sand under essentially static drained conditions. Eckersley (1990) also reported that excess pore water pressures were developed after the start of flow slides. This pore water pressure build-up was probably caused by the inability to dissipate fully the pore water pressure gener-

ated by large volumetric strain development. Therefore it can be conceived that when the effective stress reduction rate becomes equivalent to or higher than the rate at which the excess pore pressure is generated in an undrained condition, a runaway type of instability might possibly occur, even under a drained condition. It is also possible that when drained instability occurs, the amount of volumetric strain becomes so large that there is no sufficient time for the excess pore water pressure to be dissipated efficiently. The instability that has occurred initially under a drained condition may therefore evolve into a runaway instability, as has been observed by Chu *et al.* (2003) and Loke (2004) under triaxial testing conditions.

The possibility of static liquefaction or instability occurring for dilating sand has also been observed in several case studies. In a discussion to identify the mechanisms that caused the failure of the Nerlerk berm in the Canadian Beaufort Sea (Sladen *et al.*, 1985), Been *et al.* (1987) concluded that the failure could have occurred for dilatant sand. Several other cases of flow slide failure in dilatant sand have also been presented by Been *et al.* (1988). These include the failure of the Fort Peck Dam (Casagrande, 1965). Another well-documented case of a flow slide occurring in medium dense to dense sand of the Mississippi riverbanks was presented by Torrey & Weaver (1984), in which liquefaction under undrained conditions has been ruled out as the cause of failure. Casagrande (1975) described a natural phenomenon, which in the Alps is known as *Muren*, in which large masses of dense granular talus liquefy and flow down a valley, and suggested that dilation of soil was involved in the failure process. Based on Casagrande's suggestion, Fleming *et al.* (1989) have classified flow failure into contractive and dilative types. The Salmon Creek landslide in Marin County, California, which

Manuscript received 11 September 2009; revised manuscript accepted 12 April 2011. Published online ahead of print 11 November 2011. Discussion on this paper closes on 1 July 2012, for further details see p. ii.

\* Nottingham Centre for Geomechanics, Faculty of Engineering, University of Nottingham, UK.

† School of Civil and Environmental Engineering, Nanyang Technological University, Singapore, presently Department of Civil, Construction and Environmental Engineering, Iowa State University, Ames, IA, USA.

exhibited dominantly dilative transformation from solid landslide to liquid debris flow, was used by Fleming *et al.* (1989) to illustrate the different criteria that can be used in the field to distinguish contractive and dilative behaviour.

Therefore, in addition to static liquefaction of loose sand, there are other types of failure mechanism that control the stability of granular slopes. In addition to drainage conditions and density of sand, there are also other factors that contribute to the liquefaction or instability of sand, for example stress ratio, sand state, or load control mode (Chu *et al.*, 2003; Chu & Wanatowski, 2008, 2009; Wanatowski *et al.*, 2010). It should be pointed out that following the definition of Lade (1992) and Chu *et al.* (2003), the term ‘instability’ refers to a behaviour in which large plastic strains are generated rapidly, owing to the inability of a soil element to sustain a given load or stress. Liquefaction becomes a special case of instability under this definition. For this reason, instability will be used in this paper as a more general term.

The instability behaviour of loose sand is also affected by creep under either drained or undrained conditions. Lade *et al.* (1997) have shown that drained creep would have a stabilising effect on soil as far as stability is concerned. On the other hand, undrained creep in contractive sand causes the pore pressure to increase, which in turn leads the effective stress path towards, or possibly into, the zone of potential instability (Leong & Chu, 2002).

It should also be pointed out that slope failures are often caused not only by an increase in external load, but also by a reduction in the effective mean stress, for example because of water infiltration into slopes and release of lateral stress. The Aberfan coal tip disaster in the United Kingdom (Bishop, 1973) is one of the examples. Therefore, as suggested by Brand (1981) when investigating the failure mechanisms of a slope, the stress–strain behaviour of the soil along stress paths that simulate water infiltration should be studied. Such stress paths may be idealised as paths with constant shear stress, but decreasing mean effective stress, or the so-called constant shear drained (CSD) tests performed under constant deviatoric stress (Brand, 1981; Sasitharan *et al.*, 1993; Skopek *et al.*, 1994; Anderson & Riemer, 1995; Anderson & Sitar, 1995; Chu *et al.*, 2003; Orense *et al.*, 2004; Daouadji *et al.*, 2010).

Several experimental studies on pre-failure instability behaviour of sand have been reported in the past (Sasitharan *et al.*, 1993; Skopek *et al.*, 1994; Chu & Leong, 2001; Chu *et al.*, 2003; Orense *et al.*, 2004; Sento *et al.*, 2004; Daouadji *et al.*, 2010). However, all the above cited studies were carried out under axisymmetric conditions. As slopes are in plane-strain, if not in three-dimensional conditions, instability behaviour needs to be studied under plane-strain conditions. Although the behaviour of sand under plane-strain conditions has been studied before (e.g. Cornforth, 1964; Han & Vardoulakis, 1991; Finno *et al.*, 1996, 1997; Mokni & Desrues, 1998; Alshibli *et al.*, 2003; Desrues & Viggiani, 2004; Wanatowski & Chu, 2006), only a few studies have been carried out on pre-failure instability of sand under plane-strain conditions (Chu & Wanatowski, 2008, 2009; Wanatowski *et al.*, 2010). As a result, most constitutive models proposed to predict the onset of instability were only calibrated using triaxial data (e.g. Lade, 1992; Anandarajah, 1994; Wang *et al.*, 2002; Mroz *et al.*, 2003).

The objective of this paper is to examine different types of instability and identify the factors affecting the unstable behaviour of sand under plane-strain conditions using experimental data obtained from a plane-strain apparatus. The effects of stress ratio, void ratio, sand state, load control mode and reduction rate of the effective confining stress on the instability behaviour of sand are discussed and analysed in this paper using experimental data obtained from undrained instability (or creep) tests and CSD tests carried out under plane-strain conditions.

#### MATERIAL TESTED AND EXPERIMENTAL SET-UP

The sand tested is a marine-dredged silica sand used for land reclamation in Singapore. The basic properties of the sand are given in Table 1. A scanning electron micrograph of Changi sand is shown in Fig. 1. The sand grains are mainly sub-angular in shape. Since the Changi sand is dredged from the seabed, it contains shells of various sizes ranging from 0.2 to 10 mm, as shown in Fig. 1.

The drained and undrained behaviours of the sand at loose saturated state in triaxial and plane-strain compression are reported in Leong *et al.* (2000) and Wanatowski & Chu (2006, 2007). It was reported that the critical-state lines obtained from triaxial and plane-strain tests are different. The slope of the critical-state line under axisymmetric conditions (CSL<sub>tc</sub>) on the  $q-p'$  plane is  $M_{tc} = 1.35$ , which corresponds to a critical-state friction angle  $(\phi_{cs})_{tc} = 33.4^\circ$ . The slope of the critical-state line under plane-strain conditions (CSL<sub>psc</sub>) on the  $q-p'$  plane is  $M_{psc} = 1.16$ , which corresponds to a friction angle  $(\phi_{cs})_{psc} = 36.0^\circ$ . The critical-state lines on the  $e-\log p'$  plane for plane-strain and triaxial conditions are also different. However, their slopes were found to be the same, and equal to  $\lambda_{tc} = \lambda_{psc} = 0.043$  (Wanatowski & Chu, 2007). The difference in CSL for triaxial and plane-strain conditions can be explained by the dependence of  $M$  on the intermediate principal stress, in terms either of Lode's angle or of  $b$ -value, as pointed out by Jefferies & Shuttle (2002) and Wanatowski & Chu (2007).

The plane-strain apparatus developed by Wanatowski & Chu (2006) was used in this study (Fig. 2). The prismatic soil specimen was 120 mm high and 60 mm × 60 mm in

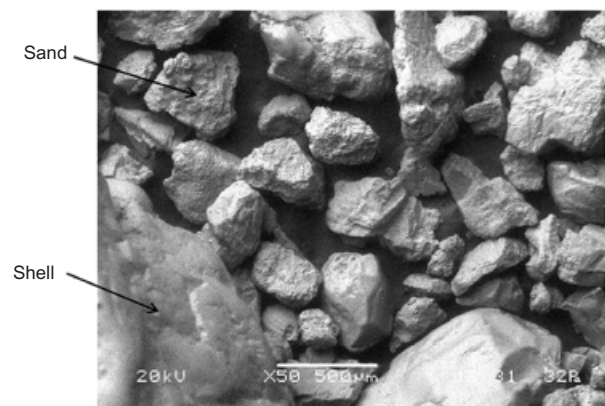
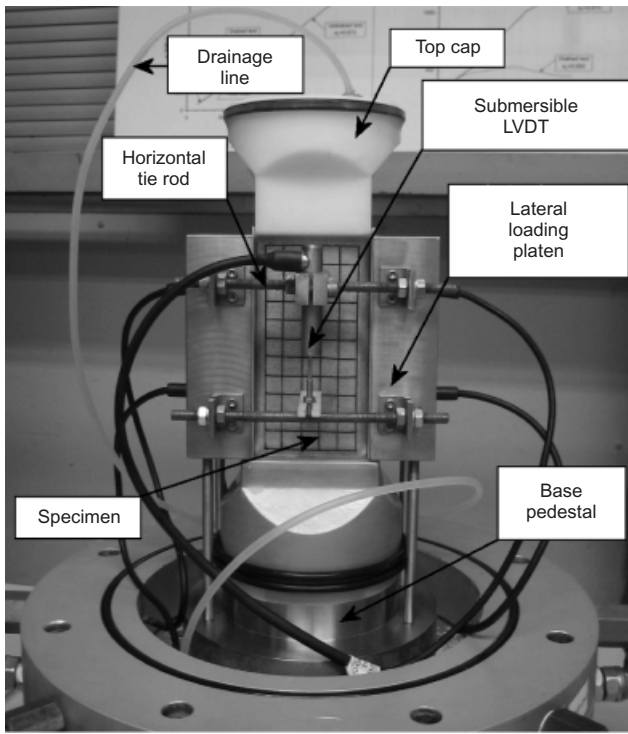


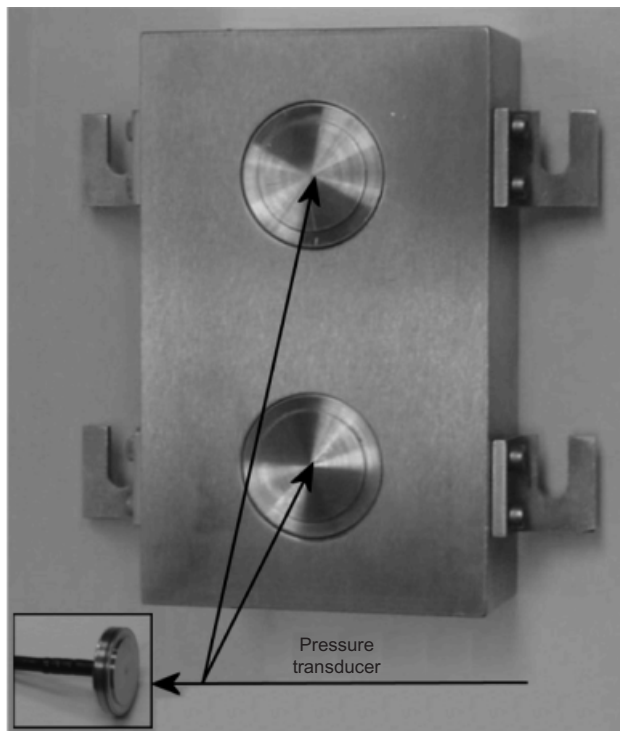
Fig. 1. Scanning electron micrograph of Changi sand

Table 1. Basic properties of the tested sand

Mean grain size: mm	Uniformity coefficient	Specific gravity	Max. void ratio	Min. void ratio	Shell content: %
0.30	2.0	2.60	0.916	0.533	12



(a)



(b)

Fig. 2. Plane-strain apparatus: (a) photograph of elevation; (b) photograph of vertical platen (after Wanatowski & Chu, 2007)

cross-section. Two stainless steel vertical platens were fixed in position by two pairs of horizontal tie rods to impose a plane-strain condition, as shown in Fig. 2(a). The intermediate principal stress ( $\sigma_2$ ) was measured by four submersible pressure transducers, with two on each vertical platen (Fig. 2(b)). The total  $\sigma_2$  was calculated as an average value obtained from the four individual transducers. The free-end technique (Rowe & Barden, 1964) was used to reduce the

boundary friction, and to delay the occurrence of non-homogeneous deformations. For this purpose, all the platens were enlarged. High-vacuum silicone grease was applied to all the rigid surfaces. For the top and base platens, latex discs were used. For the two lateral platens, Teflon sheets were adapted. A pair of miniature submersible linear variable differential transformers (LVDTs) was used to measure the vertical displacement (Fig. 2(b)). An external LVDT was also used to measure the axial strain when the internal LVDTs ran out of travel. A digital hydraulic force actuator was mounted at the bottom of a loading frame to apply axial load. The actuator was controlled by a computer by way of a digital load/displacement control box. The control box adjusted the movement of the base pedestal to achieve a desired rate of load or rate of displacement so that the plane-strain apparatus could be used under either deformation-controlled or load-controlled loading mode. The cell pressure was applied through a digital pressure/volume controller (DPVC). Another DPVC was used to control the back-pressure from the bottom of the specimen while measuring the volumetric change at the same time. A pore pressure transducer was used to record the pore water pressure at the top of the specimen. For details of the testing arrangement, see Wanatowski & Chu (2006, 2007).

Laboratory reconstituted specimens were prepared by either the water sedimentation (WS) or the moist tamping (MT) method. The WS method was used for medium loose and medium dense samples, and the MT method was used to prepare very loose specimens. A liquid rubber technique (Lo *et al.*, 1989) was adopted to reduce the effect of membrane penetration. All the specimens were saturated by flushing with de-aired water from the bottom to the top for a period of 60 min. A back-pressure of 400 kPa was also applied. For all the specimens, the  $B$ -value (Skempton's pore water pressure parameter) achieved was in the range 0.96–0.98. The void ratio after saturation was back-calculated based on the water content of the specimen at the end of a test and the volume changes during consolidation and shearing, a procedure proposed by Verdugo & Ishihara (1996).

All the plane-strain specimens were  $K_0$  consolidated. The  $K_0$  condition was imposed by regulating the volume change of the specimen in accordance with the axial strain to maintain  $d\varepsilon_v/d\varepsilon_1 = 1$ , a method described by Lo & Chu (1991).

In this study, the deviatoric stress  $q$  and the mean effective stress  $p'$  under plane-strain conditions are defined as

$$q = \frac{1}{\sqrt{2}} [(\sigma_1 - \sigma_2)^2 + (\sigma_2 - \sigma_3)^2 + (\sigma_3 - \sigma_1)^2]^{1/2} \quad (1)$$

$$p' = \frac{1}{3} (\sigma'_1 + \sigma'_2 + \sigma'_3) \quad (2)$$

where  $\sigma_1$ ,  $\sigma_2$  and  $\sigma_3$  are the major, intermediate and minor principal stresses respectively, and the prime refers to effective stress.

### TYPES OF INSTABILITY

#### *Instability under undrained conditions*

It is well known that when loose sand specimens are sheared in a triaxial cell under undrained conditions, the effective stress paths shown in Fig. 3 will be obtained. If the test is conducted under a load-controlled condition, the specimen will become unstable at the peak point. This behaviour has often been referred to as *static liquefaction*. The line that connects the top of the effective stress paths has been called the *instability line* (Lade, 1992), as shown in Fig. 3. The *critical-state line* (CSL), which is also the failure line for loose sand as determined by drained triaxial tests, is

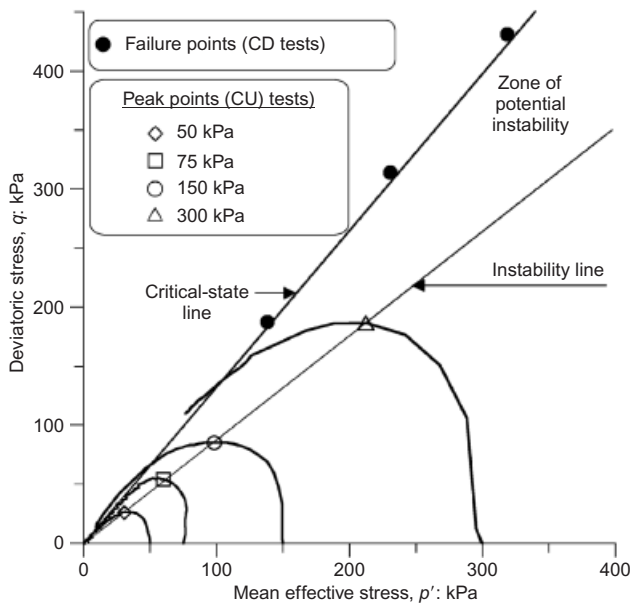


Fig. 3. Definition of instability line and zone of potential instability based on CIU triaxial tests on loose sand

also shown in Fig. 3. The zone between the instability line and the CSL is called the *zone of potential instability*; it specifies the instability condition for loose sand under undrained conditions (Lade, 1992). However, if an undrained test is conducted on loose sand under a deformation-controlled loading condition, static liquefaction or instability in the form of a sudden increase in axial strain rate will not occur. In this case, strain-softening in the form of a reduction in the deviator stress occurs instead. For more discussion, see Chu & Leong (2001) and Chu & Wanatowski (2009).

The findings mentioned above are established under axisymmetric conditions using triaxial tests. However, Wanatowski & Chu (2007) showed that the instability line can also be established under plane-strain conditions. Fig. 4 presents the effective stress paths (Fig. 4(a)) and corresponding stress-strain curves (Fig. 4(b)) of the three  $K_0$  consolidated undrained plane-strain tests conducted on very loose sand. It can be seen from Fig. 4(a) that a line can be drawn through the peak points of the undrained stress paths in a way similar to that shown in Fig. 3. It has been established by Wanatowski & Chu (2007) that this line defines the instability line of sand under plane-strain conditions, and can be used in the same way as the instability line defined under axisymmetric conditions to specify the conditions for instability under plane-strain conditions.

Figure 5 presents the results of two instability tests, INU01 and INU03, carried out on loose sand specimens with void ratios  $e_c$  of 0.907 and 0.894 respectively. The two tests were carried out in a similar way. Test INU01 was performed by shearing the specimen from the  $K_0$  condition (point  $A_1$ ) to an effective stress ratio of  $q/p' = 1.04$  (point  $B_1$ ) along a drained path, as shown in Fig. 5(a). Test INU03 was sheared from the  $K_0$  condition (point  $A_3$ ) to point  $B_3$  along a drained path. The deviatoric stress at point  $B_3$  is the same as that in Test INU01 ( $q = 190$  kPa). However, in terms of effective stress ratio,  $q/p'$  at point  $B_3$  is 0.96, which is lower than that at point  $B_1$  for Test INU01. The void ratios at points  $B_1$  and  $B_3$  were 0.889 and 0.886 respectively. Upon reaching points  $B_1$  and  $B_3$  an undrained condition was imposed, while the deviatoric stress was maintained constant in both tests.

The excess pore water pressure and the axial strain

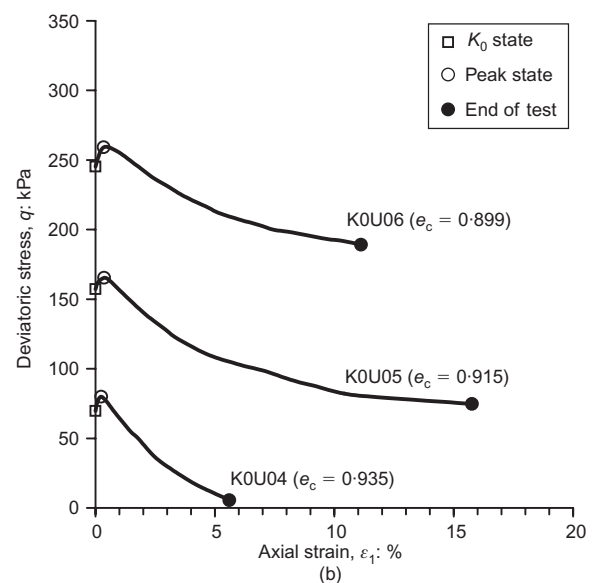
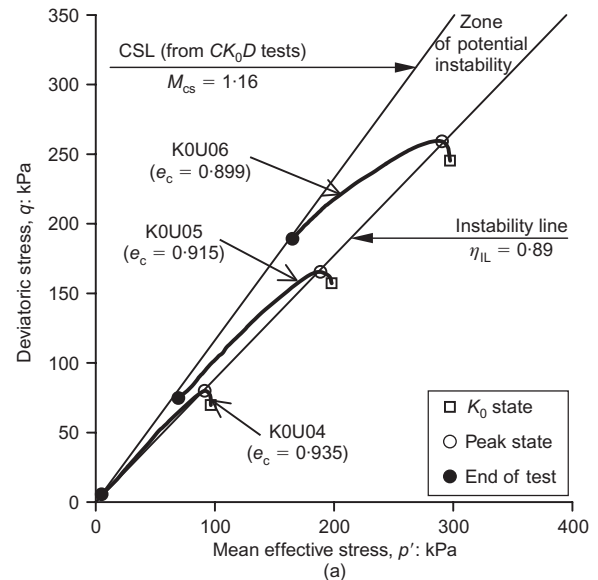


Fig. 4. Definition of instability line and zone of potential instability based on  $CK_0U$  plane-strain tests on very loose sand: (a) effective stress paths; (b) corresponding stress-strain curves

development during the instability tests are shown in Figs 5(b) and 5(c) respectively. It can be seen from Fig. 5(b) that in Test INU01 the pore water pressure started to increase immediately after drainage conditions were changed from drained to undrained at point  $B_1$ . Within the next few minutes the pore water pressure shot up, and instability occurred at point  $C_1$ . This was accompanied by a sudden increase in axial strain rate, as shown in Fig. 5(c). The effective stress at point  $C_1$  is shown in Fig. 5(a). It can be seen that  $C_1$  is on the IL. When instability occurred, the specimen physically collapsed. Test INU03 was carried out in a way similar to Test INU01, except that the consolidation stresses were higher. Upon reaching point  $B_3$ , the deviatoric stress was kept constant and an undrained condition was imposed. In Test INU03, however, the pore water pressure and the axial strain did not change much under an undrained condition (Figs 5(b) and 5(c)). The specimen was at a stable state.

The IL corresponding to  $e = 0.888$  as determined by the  $CK_0U$  plane-strain tests conducted on very loose sand (Wanatowski & Chu, 2007) is also plotted in Fig. 5(a). It can be seen that the IL determined by the  $CK_0U$  tests

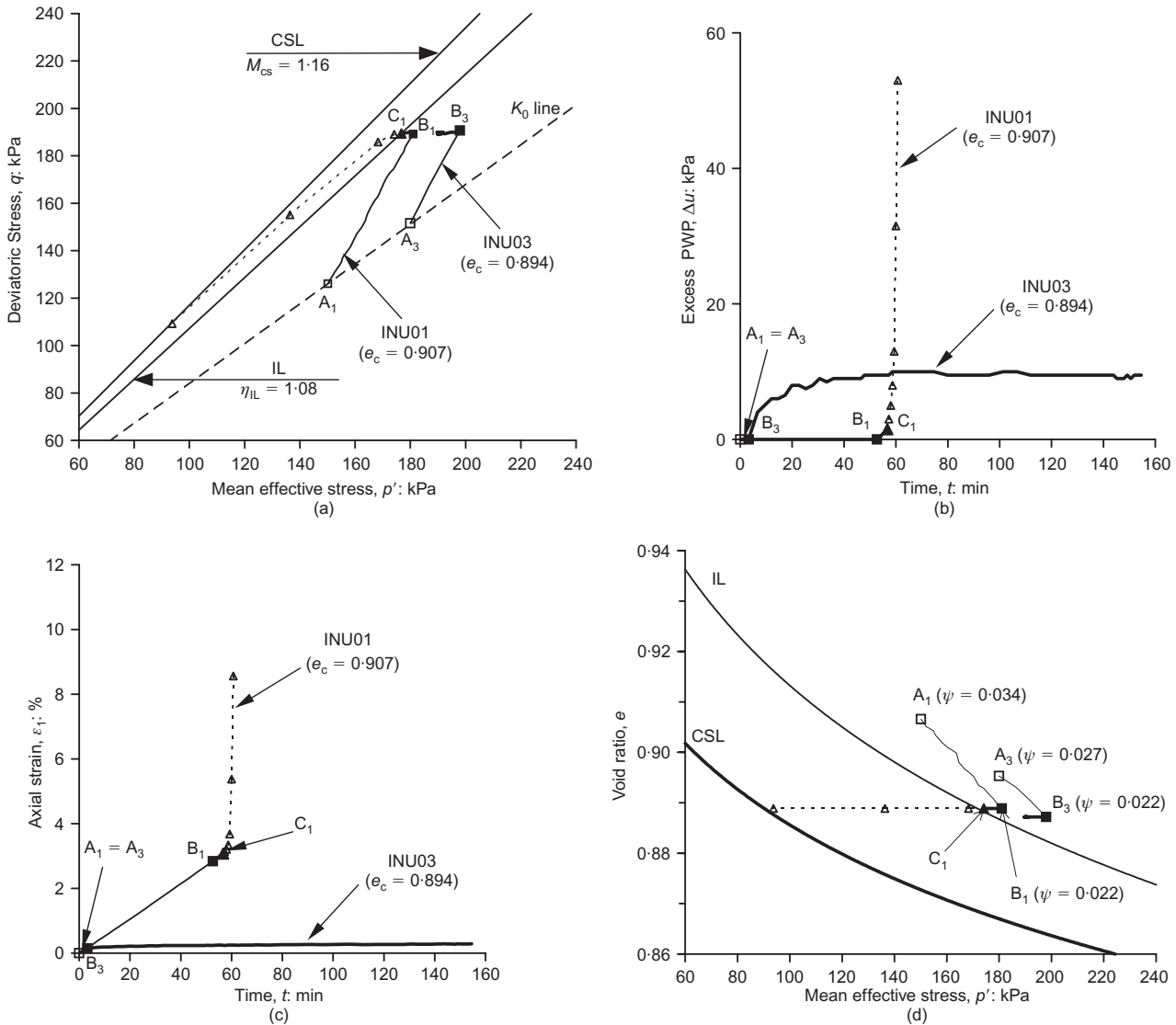


Fig. 5. Instability of loose sand under undrained condition: (a) effective stress paths; (b) excess pore water pressure against time; (c) axial strain against time; (d)  $e-p'$  plot

coincides with point C<sub>1</sub> where the specimen in Test INU01 became unstable under load-controlled conditions. It can therefore be concluded that stress ratio affects the occurrence of pre-failure instability of loose sand under undrained, plane-strain conditions. Instability occurs if the stress point is on or above its instability line.

The  $e-p'$  plot of the two tests is presented in Fig. 5(d). The IL and CSL are plotted in the figure. The state parameters  $\psi$  (Been & Jefferies, 1985) at points A<sub>1</sub>, B<sub>1</sub> and A<sub>3</sub>, B<sub>3</sub> of Tests INU01 and INU03 respectively are also indicated in Fig. 5(d). The state parameter is defined as

$$\psi = e_0 - e_{cs} \quad (3)$$

where  $e_0$  is the void ratio at the initial state and  $e_{cs}$  is the void ratio at the critical state at the same mean effective stress,  $p'$ .

It can be observed from Fig. 5(d) that the IL on the  $e-p'$  plane coincides with point C<sub>1</sub> where the specimen in Test INU01 became unstable under load-controlled conditions. Once the instability occurred, the mean effective stress reduced quickly towards the CSL. The specimen in Test INU03, however, was at a stable state, even though the state parameter at point B<sub>3</sub> ( $\psi = 0.022$ ) was identical to that at point B<sub>1</sub> in Test INU01. It can therefore be concluded that the instability occurs if the soil state reaches the instability line on both the  $q-p'$  (Fig. 5(a)) and  $e-p'$  (Fig. 5(d)) planes.

This condition may not necessarily be captured by the state parameter  $\psi$ , which defines the distance (in terms of void ratio) between the soil state and the CSL but not the distance between the soil state and the IL, as indicated in Fig. 5(d).

Figure 5 also demonstrates the effect of undrained creep on the instability behaviour of loose sand. It can be seen from Fig. 5(a) that point B<sub>1</sub> in Test INU01 was below the instability line. Therefore instability should not occur under this condition. Instability indeed did not occur at point B<sub>1</sub>. However, when the stress path of Test INU01 reached point C<sub>1</sub>, which was within the zone of instability, instability occurred in the form of a rapid increase in pore water pressure and axial strain, as shown in Figs 5(b) and 5(c). The results of Test INU01 have therefore indicated that, even when the initial stress state is below the instability line, instability can still occur if creep is developing under an undrained condition. This is because the stress state will move to the left on the  $q-p'$  plane when the pore water pressure develops because of undrained creep, as shown in Fig. 5(a). If the stress point is below, but very close to, the instability line, such as point B<sub>1</sub> in Fig. 5(a), undrained creep may cause the effective stress to move towards the instability zone. When the effective stress path goes beyond the instability line, instability will occur.

On the other hand, if the initial stress state is not very

close to the instability line, such as point B<sub>3</sub> in Fig. 5(a), the pore water pressure will stop increasing with time after it has reached a maximum value, as shown in Fig. 5(b). In this case, instability will not occur even when undrained creep has developed. The value of the maximum pore water pressure depends on the stress state at which creep takes place and the void ratio of the soil, as discussed in detail by Leong & Chu (2002).

*Instability under drained conditions*

It has been established by several researchers (Lade *et al.*, 1987; Lade & Pradel, 1990; Leong *et al.*, 2000; Chu *et al.*, 2003) that pre-failure instability will not occur for loose or dense sand under a drained condition if the stress state imposed into a soil element does not change. Therefore it is commonly believed that the soil behaviour is stable under a fully drained condition. However, soil can become unstable along a certain stress path. For example, during water infiltration, a soil element in a slope may follow a CSD stress path, as suggested by Brand (1981). Along this stress path, a soil element may become unstable under fully

drained conditions (Sasitharan *et al.*, 1993; Skopek *et al.*, 1994; Anderson & Riemer, 1995; Anderson & Sitar, 1995; Chu *et al.*, 2003; Leong, 2004; Loke, 2004; Wanatowski, 2005; Wanatowski *et al.*, 2010).

Data on drained instability under axisymmetric conditions have been shown by Chu *et al.* (2003). Similar observation is also made under plane-strain conditions. The results of a typical drained instability test under plane-strain conditions, IND01, are shown in Fig. 6. The loose sand specimen (with a void ratio  $e_c = 0.902$ ) was first  $K_0$ -consolidated to the mean effective stress of 200 kPa (point A<sub>1</sub>), as shown in Fig. 6(a). The deviatoric stress at point A<sub>1</sub> is  $q = 173$  kPa (Figs 6(a) and 6(b)). After consolidation, the specimen was sheared along the CSD path with the deviator load maintained constant. On the CSD path, the confining stress ( $\sigma_3$ ) was reduced by increasing the back-pressure at a rate of 0.5 kPa/min, resulting in a stress path moving from point A<sub>1</sub> to point I<sub>1</sub> (Fig. 6(a)) and the effective stress ratio  $q/p'$  increasing from 0.87 to 1.05. There was little axial and volumetric strain development until point I<sub>1</sub> where both strains started to develop at a faster rate, indicating an unstable behaviour, as shown in Fig. 6(c). Using point I<sub>1</sub>,

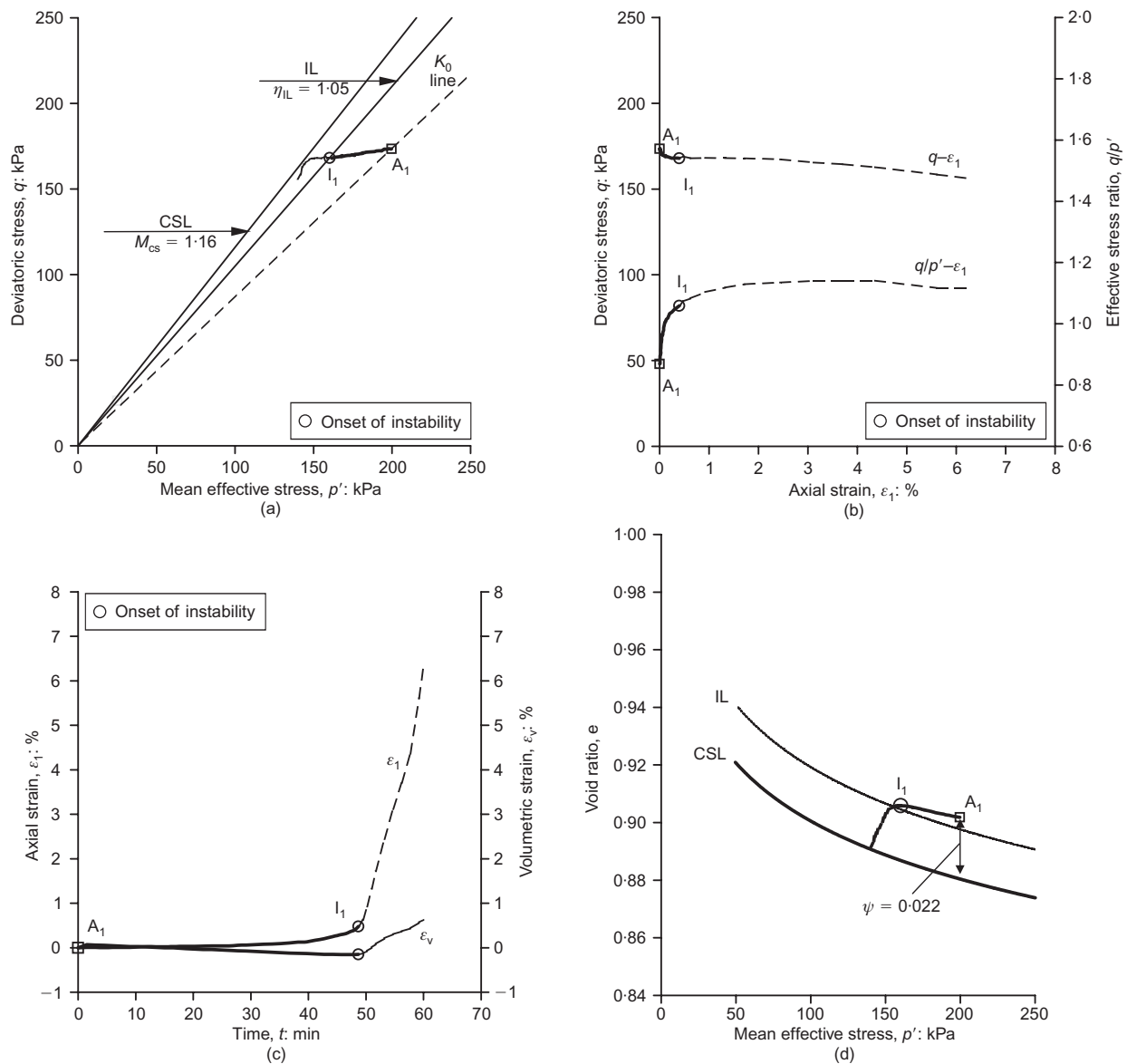


**Fig. 6.** Instability of loose sand under drained condition (Test IND01,  $e_c = 0.902$ ): (a) effective stress path; (b) deviatoric stress and effective stress ratio against axial strain; (c) axial strain and volumetric strain against time; (d)  $e-p'$  plot

the instability line can be determined, as shown in Fig. 6(a). The gradient of the IL,  $\eta_{IL}$ , is 1.05. This is smaller than the gradient of the CSL,  $M_{cs} = 1.16$ . Thus instability observed in Test IND01 is a pre-failure instability. As shown in Fig. 6(a), with further reduction in the confining stress, the stress path moved further towards the CSL. However, at this stage the axial and volumetric strain rates had increased to such an extent that the testing system could not maintain deviator load to be constant. It needs to be pointed out that the pore water pressure did not change during the whole test. Therefore the instability in the form of a rapid increase in plastic strains was observed in Test UND01 under a fully drained condition.

The  $e-p'$  plot of Test IND01 is presented in Fig. 6(d). It can be observed from Fig. 6(d) that instability occurred upon reaching the instability line. Similar to the effective stress path on the  $q-p'$  plane (Fig. 6(a)), once instability occurred at point  $I_1$ , the path on the  $e-p'$  plane moved towards the CSL, with further reduction in the mean effective stress  $p'$ .

## FACTORS AFFECTING PRE-FAILURE INSTABILITY

### Stress ratio

The occurrence of undrained instability is affected by the stress ratio. This has been shown by previous studies under axisymmetric conditions (Lade, 1993; Leong *et al.*, 2000; Leong & Chu, 2002). This has also been shown to be the case in Fig. 5 under plane-strain conditions.

The effect of stress ratio on the pre-failure instability of loose sand is related to the conditions for large plastic yielding to develop. For plastic flow to develop, the yield surface has to expand, which requires the stress increment to point outside the yield surface. The effective stress path involved in an instability test is characterised by  $dq \leq 0$  and  $dp' < 0$ . The deviator stress  $q$  decreases because the cross-section of the specimen increases while the deviator load is maintained constant. The effective mean stress decreases owing to the increase in pore pressure. As discussed by Chu & Leong (2001), such a stress path points outside the yield surface only when a stress ratio is higher than the stress ratio at the peak point of the yield surface. If the stress ratio where an instability test starts is lower than the stress ratio at the peak point, such a stress path will point inside the yield surface and result in an elastic response. These conditions are approximately defined by the instability line shown in Figs 3 and 4. Therefore the instability line is associated with the yield surface, and defines the conditions under which large plastic yielding can take place (Lade, 1992; Chu *et al.*, 1993; Imam *et al.*, 2002). Large plastic yielding has to take place when soil becomes unstable: that is, when large plastic strain develops rapidly. Therefore yielding is a necessary condition for instability.

However, the yielding condition does not specify drainage conditions. Therefore the zone of potential instability should define the conditions of instability, regardless of the drainage condition. Thus the zone of instability also specifies the conditions for drained instability. This has been shown to be the case under axisymmetric conditions by Chu *et al.* (2003) and under plane-strain conditions by the data shown in Fig. 6. Using more testing data (Chu *et al.*, 2003; Loke, 2004; Wanatowski, 2005; Wanatowski & Chu, 2007; Chu & Wanatowski, 2008; Wanatowski *et al.*, 2010), the relationship between the slope of instability line and the void ratio can be established under both axisymmetric and plane-strain conditions, as shown in Fig. 7. This finding has important practical implications. It implies that pre-failure instability can occur under both drained and undrained conditions and the necessary conditions for undrained and drained instability are the same. This explains why liquefaction under

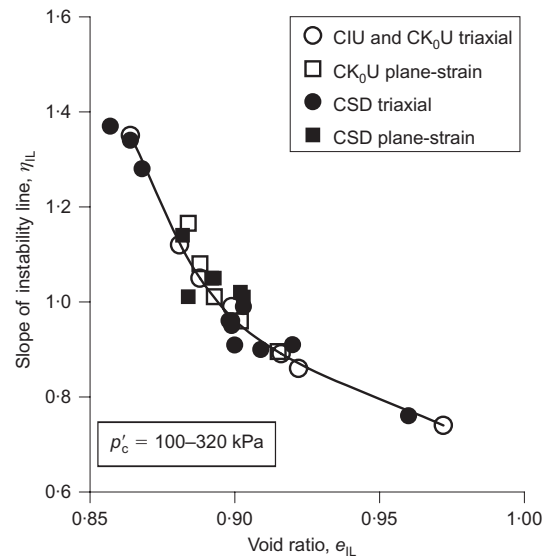


Fig. 7. Relationship between slope of instability line and void ratio established from triaxial and plane-strain tests

complete drained conditions had occurred in the Wachuset dam failure (Olson *et al.*, 2000); that is, because a stress path led the stress state into the zone of potential instability. Such a path can be applied to both loose and dense sand. Thus both loose and dense sand can become unstable under drained conditions. When a loose sand is sheared under undrained conditions, the pore water pressure will increase and lead an effective stress path into the zone of potential instability. When a dense sand is sheared under undrained conditions, the pore water pressure reduces and the resulting effective stress moves away from the zone of instability, and thus instability does not occur.

### Void ratio

As explained earlier, under undrained conditions, pre-failure instability occurs for loose sand only. However, under drained conditions, pre-failure instability can occur for both loose and dense sand. The results of two plane-strain tests, IND01 and IND03, are presented in Fig. 8, to discuss the effect of void ratio on the pre-failure instability behaviour. Tests IND01 and IND03 were conducted on very loose and medium dense sand respectively. The specimens in the two tests were anisotropically consolidated to mean effective stresses of 200 kPa and 206 kPa (points  $A_1$  and  $A_3$ ). The void ratios of the specimens after consolidation were  $e_c = 0.902$  and  $0.679$  respectively. After consolidation, the specimens were sheared along CSD paths. The effective stress paths obtained from the two tests are plotted in Fig. 8(a). The critical-state line (CSL) and the failure line (FL) as defined by drained plane-strain tests (Wanatowski & Chu, 2006) are also plotted in Fig. 8(a). It can be seen that, owing to the reduction in the mean effective stress, the effective stress paths moved from points  $A_1$  and  $A_3$  to points  $I_1$  and  $I_3$  respectively. The changes in axial strain and axial strain rate with time for the two tests are presented in Fig. 8(c). It can be seen from Fig. 8(c) that between points  $A_1$ ,  $A_3$  and  $I_1$ ,  $I_3$  there was little axial strain developed in both tests. The two specimens in Tests IND01 and IND03 underwent an axial deformation of approximately 0.32% and 0.44% respectively. This can be seen more clearly from the stress-strain curves plotted in Fig. 8(b). When the stress states reached points  $I_1$  and  $I_3$ , the axial strains in both tests started to develop at faster rates, as shown in Fig. 8(c). According to the definition given by Chu *et al.* (2003),

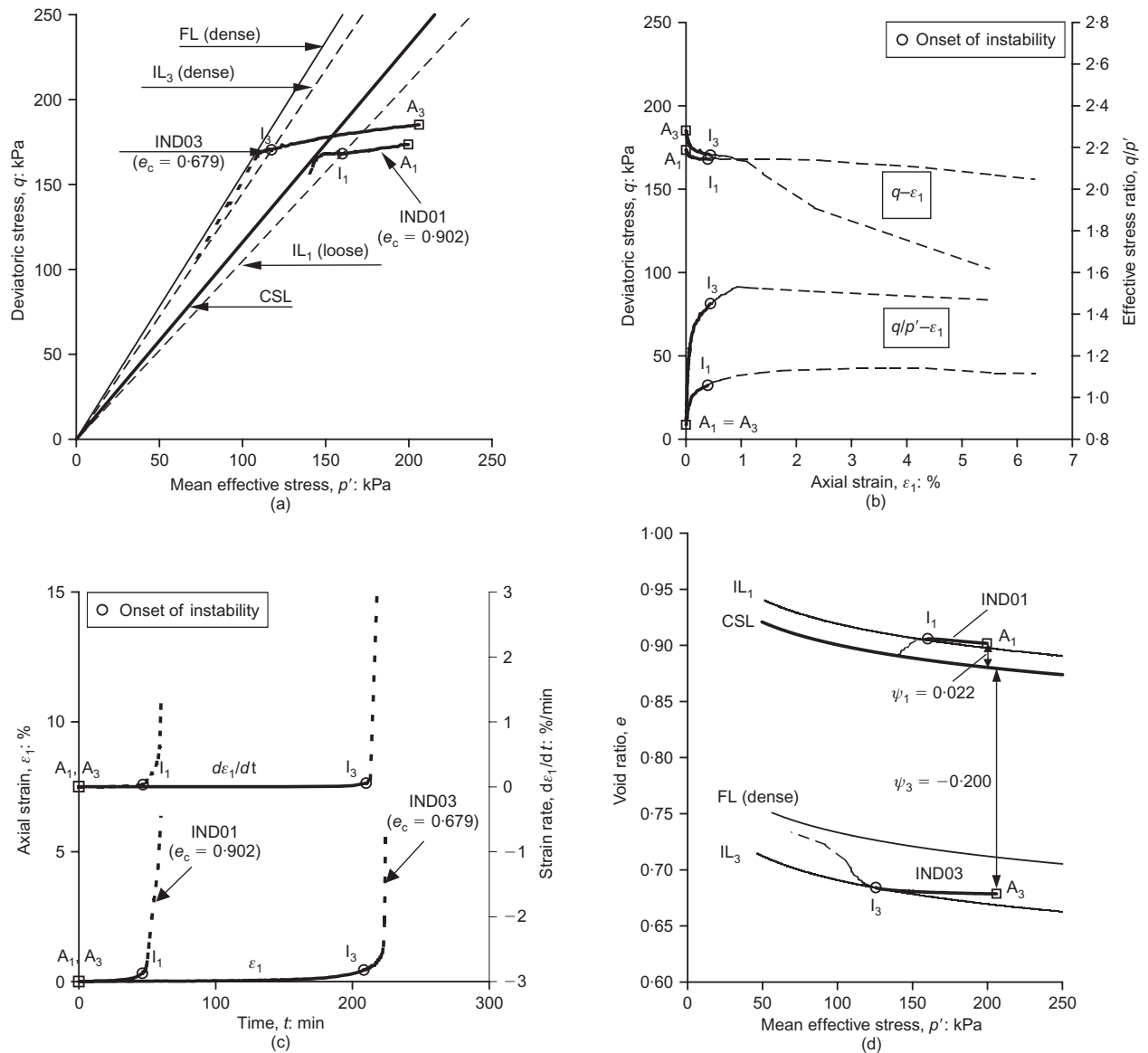


Fig. 8. Effect of void ratio on instability of sand under drained conditions: (a) effective stress paths; (b) deviatoric stress and effective stress ratio against axial strain; (c) axial strain and volumetric strain against time; (d)  $e-p'$  plots

instability occurred at points I<sub>1</sub> and I<sub>3</sub>. This means that drained instability can occur for both loose and dense sand. After the occurrence of instability, the stress-strain curves of the two tests do not represent the element behaviour any more, as illustrated by the dashed lines in Fig. 8(b).

Although the instability occurred for both loose and dense sand, the conditions at which instability occurred were different. The instability lines (IL) for both the loose and dense specimens can be determined using the onset of instability points I<sub>1</sub> and I<sub>3</sub> respectively, as shown in Fig. 8(a). The gradient of the IL,  $\eta_{IL}$ , obtained from Test IND01 is 1.05, whereas the gradient of the IL obtained from Test IND03 is 1.45 (Fig. 8(a)). Thus the stress ratio required for instability to occur is much smaller for very loose specimens than that for medium dense specimens, as illustrated by the  $q/p'-\varepsilon_1$  curves in Fig. 8(b). It is well known that loose granular slopes are more susceptible to instability. The test data presented in Fig. 8(a) provide a way to specify the susceptibility to instability in a quantitative way.

The drained instability observed in both tests is pre-failure instability. The very loose specimen became unstable before reaching the CSL, which is the failure line for very loose sand. On the other hand, the medium dense specimen

became unstable after the CSL, but still before reaching the failure line determined by drained plane-strain compression tests on medium dense sand (Wanatowski & Chu, 2006, 2007).

The  $e-p'$  plot of the two tests is presented in Fig. 8(d). It can be observed from Fig. 8(b) that instability in both tests occurred upon reaching two different instability lines, IL<sub>1</sub> (very loose sand) and IL<sub>3</sub> (medium dense sand).

#### Soil state

The experimental data presented above have shown that the occurrence of instability under plane-strain conditions depends on the stress ratio and the void ratio of soil. In other words, the occurrence of instability depends on the state of soil.

As described earlier, the state parameter  $\psi$  is often used to describe the initial state of soil in terms of the difference between the initial state after consolidation and the critical state in the  $e-p'$  plane (Been & Jefferies, 1985). Several researchers have related instability conditions to the state parameter (Sladen *et al.*, 1985; Anderson & Riemer, 1995; Yang, 2002). However, as observed by Chu *et al.* (2003) and

Wanowski *et al.* (2010), the state parameter concept may not be used directly for prediction of the instability behaviour of sand. This is because the state parameter defined in equation (3) is normally determined with respect to the void ratio of the soil after consolidation. For instance, the soil states at points B<sub>1</sub> (Test INU01), B<sub>3</sub> (Test INU03) and A<sub>1</sub> (Test IND01), shown in Figs 5(a) and 6(a) respectively, are characterised by the same state parameter  $\psi = 0.022$ . However, instability has occurred in Tests INU01 and IND01, but not in Test INU03. Furthermore, Wanowski *et al.* (2010) have shown that even if the state parameters  $\psi$  of two specimens are different, instability can occur upon reaching the same instability line. Therefore it can be concluded that the  $\psi$  is not suitable for the interpretation of slope stability in granular soils. To facilitate application to slope stability analysis, a modified state parameter  $\bar{\psi}$  was proposed by Chu *et al.* (2003) as

$$\bar{\psi} = e_{IL} - e_{cs} \quad (4)$$

where  $e_{IL}$  is the void ratio at the instability state and  $e_{cs}$  is the void ratio at the critical state under the same mean effective stress,  $p'$ .

The relationship between the slope of the instability line  $\eta_{IL}$  and the modified state parameter  $\bar{\psi}$  is plotted in Fig. 9 using all the test data presented previously in Fig. 7. Note that  $\eta_{IL}$  is normalised by the slope of the CSL,  $M_{sc}$ . This normalisation is necessary because the CSL determined under plane-strain test conditions is different from that under axisymmetric conditions (Wanowski & Chu, 2006). The difference in CSL is related to the effect of the intermediate principal stress, as discussed by Jefferies & Shuttle (2002) and Wanowski & Chu (2007). Therefore the  $\bar{\psi}$  (or  $\psi$ ) value for plane-strain tests is different from that for triaxial tests for soil with the same void ratio and mean effective stress. Consequently, two different  $\eta_{IL}-\bar{\psi}$  curves are obtained for triaxial and plane-strain data (Wanowski *et al.*, 2010). If  $\eta_{IL}$  is normalised using the slope of the CSL,  $M_{sc}$ , and plot  $\eta_{IL}/M_{sc}$  against  $\bar{\psi}$ , a single curve can be obtained, as shown in Fig. 9. Therefore a unique relationship between  $\eta_{IL}/M_{sc}$  and  $\bar{\psi}$  exists for both plane-strain and triaxial tests. This relationship implies that the framework of the instability line for sand established under axisymmetric conditions can be extended to plane-strain conditions when the general-

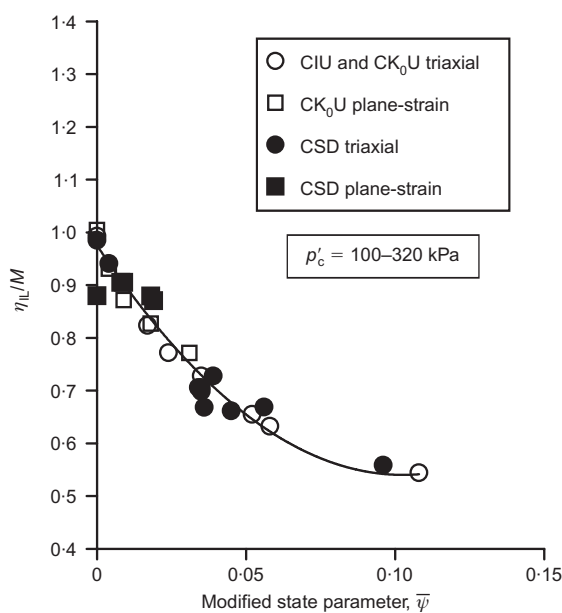


Fig. 9. Relationship between slope of instability line and modified state parameter established from triaxial and plane-strain tests

ised stress parameters are used in calculating the effective stress ratio,  $\eta$ .

The experimental data presented in Fig. 9 are consistent with theoretical and analytical investigations published in the literature (Pradel & Lade, 1990; Lade, 1992; Imam *et al.*, 2002; Chu *et al.*, 2003; Been & Jefferies, 2004; Andrade, 2009). In these studies it has been established that instability of granular materials depends on the state of the soil, although slightly different interpretations have been given by different researchers. As a result, the frameworks used to specify the instability conditions are different. Nevertheless, the physical meaning behind the different interpretations is essentially the same: that is, to predict a yielding state where large plastic strains can develop. For example, Pradel & Lade (1990) demonstrated that instability occurs below the failure line when certain kinematic conditions are present: that is, where the yield surface opens up and the granular material tends to compress. Lade (1992, 1993) further demonstrated that these conditions can be specified by the instability line, which defines the stress state located very close to the top of the yield surface. Been & Jefferies (2004) argued that the mobilised stress ratio at the onset of instability ( $\eta_{IL}$ ) does not have any physical significance for modelling soil liquefaction. They suggested that instability could be related to a change in a hardening modulus rather than the frictional properties of soil defined by the peak shear stress. Andrade (2009) confirmed that the occurrence of instability can indeed be predicted as a function of the soil state, and is associated with a limiting hardening modulus. In other words, the slope of the instability line is a function of the hardening modulus, which in turn is a function of the soil state.

#### Drainage conditions

It has been shown in preceding sections that pre-failure instability can occur for loose sand under either an undrained or a drained condition. The question then arises as to what the role of drainage is in affecting the instability behaviour. First, it should be pointed out that the instability occurring under drained conditions is different from that under undrained conditions. The strain rates developed during the two types of instability are different. The instability that occurs under undrained conditions is a 'runaway' type, and the specimen collapses almost instantly. The strain rate developed during a drained instability may be affected by the mean stress reduction rates adopted in conducting a CSD test.

To investigate the effect of the mean effective stress reduction rate, five plane-strain tests on very loose sand were conducted using  $\sigma'_3$  reduction rates of 0.25, 0.50, 1.00, 3.00 and 5.00 kPa/min, as shown in Fig. 10(a). Similar tests were also carried out on medium dense specimens (Wanowski, 2005). The effective stress paths resulted from the five tests are plotted in Fig. 10(b). All the tests were  $K_0$ -consolidated to the effective stress ratio  $q/p' = 0.88$  (points A, B, C, D and E). After that, a deviator load was maintained constant and a back-pressure was increased with a constant rate. As a result, the effective confining stress,  $\sigma'_3$ , was reduced at a constant rate (Fig. 10(a)). From the effective stress paths in Fig. 10(b) it can be seen that although the effective confining pressures of the five tests were reduced at different rates during the instability tests, all the specimens became unstable at the stress states located on the same instability line (points A', B', C', D' and E'). The gradient of the IL is  $\eta_{IL} = 1.05$ . This observation clearly demonstrates that the effective stress path is independent of the reduction rate, or, in other words, that the reduction rate does not affect the occurrence of instability. However, the times taken by the

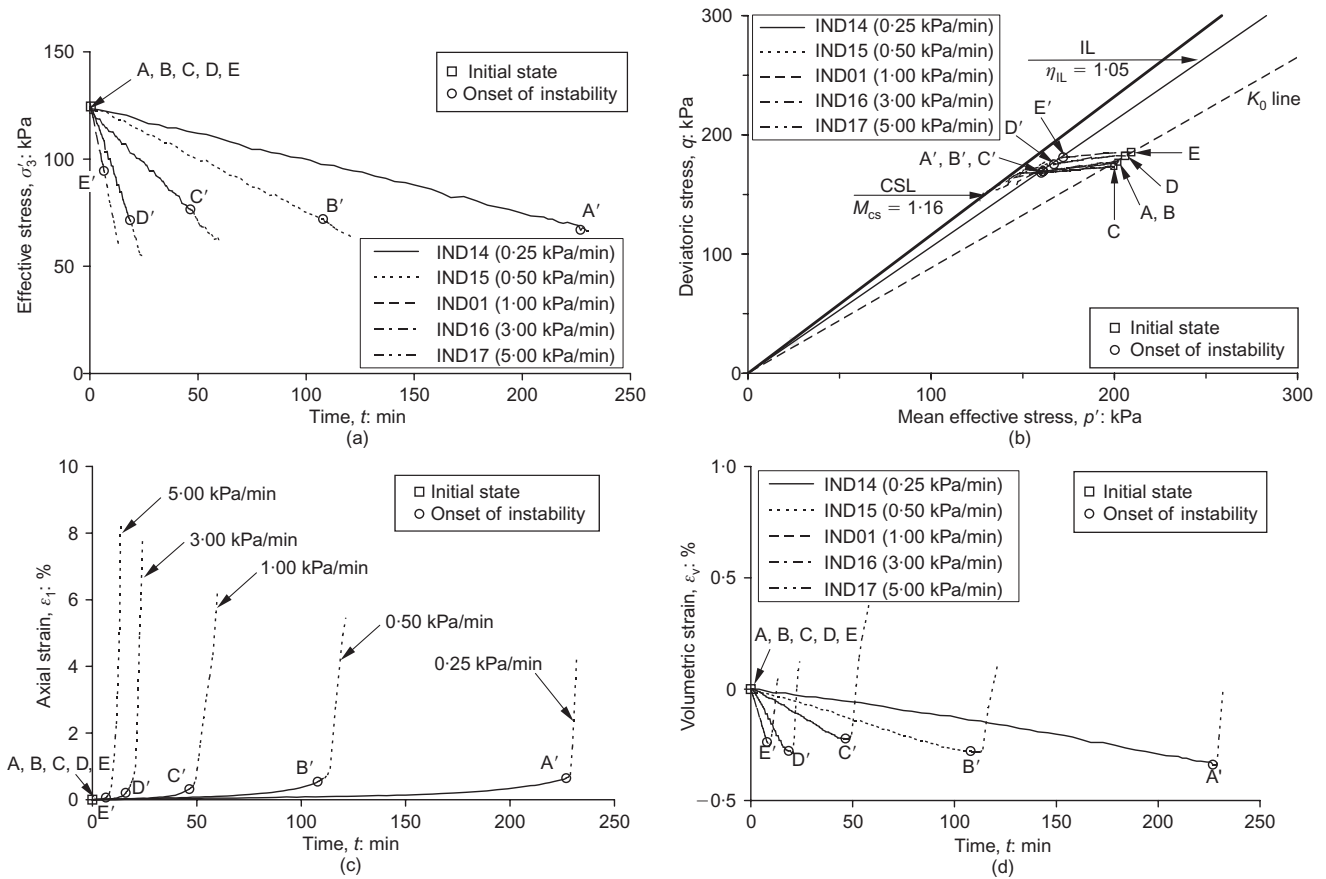


Fig. 10. Effect of  $\sigma'_3$  reduction rate on instability of very loose sand: (a)  $\sigma'_3$  against time; (b) effective stress paths; (c) axial strain against time; (d) volumetric strain against time

five specimens to reach the IL were different. From the curves of axial strain against time presented in Fig. 10(c) it can be seen that the amount of time taken for instability to occur becomes shorter as the reduction rate increases. A similar observation can be made based on the curves of volumetric strain against time shown in Fig. 10(d).

The relationships between the time taken to instability and the  $\sigma'_3$  reduction rate used for both very loose and medium dense sand are plotted in Fig. 11. It can be seen that there is a significant reduction in the time taken for instability to occur when the  $\sigma'_3$  reduction rate was increased from 0.25 kPa/min to 1.0 kPa/min. However, an increase in the

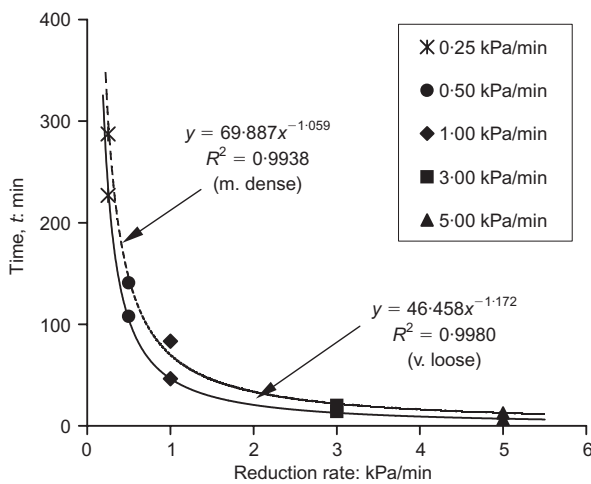


Fig. 11. Relationship between duration of CSD test and  $\sigma'_3$  reduction rate

reduction rate beyond 1.0 kPa/min does not influence the time taken significantly. This behaviour was consistent for all the very loose and medium dense specimens (Wanatowski, 2005). The relationship between the axial strain at the onset of instability and the reduction rate is plotted in Fig. 12. It can be seen that less axial deformation is developed during the CSD test with increasing reduction rate.

The relationships shown in Figs 11 and 12 imply that when the effective stress reduction rate is very high, instability can occur very quickly, with a small axial strain developed up to the onset of instability. Furthermore, after instability is initiated, the axial strain develops very rapidly too (see Fig. 10(c)). Such behaviour is very similar to the runaway instability that occurs for loose sand under undrained conditions.

The relationships between the axial strain rate developed during instability and the effective stress reduction rates for very loose and medium dense sand are presented in Fig. 13. Exponential relationships were obtained for both densities. It can be seen that the axial strain rate increases with increasing  $\sigma'_3$  reduction rate. These relationships imply that when the stress reduction rate is large enough, the axial strain rate can be as high as that in a runaway type of instability. There can be two extreme cases. The first is when there is no change in the mean effective stress. In this case, the strain rate does not increase, and instability will not occur under drained conditions, as observed by Lade *et al.* (1987), Lade & Pradel (1990) and Leong *et al.* (2000). The second is when the effective stress reduction rate is sufficiently high, and a runaway instability will occur in a drained test. Therefore it can be concluded that instability under drained conditions can only take place along a CSD path where the mean effective stress is reducing.

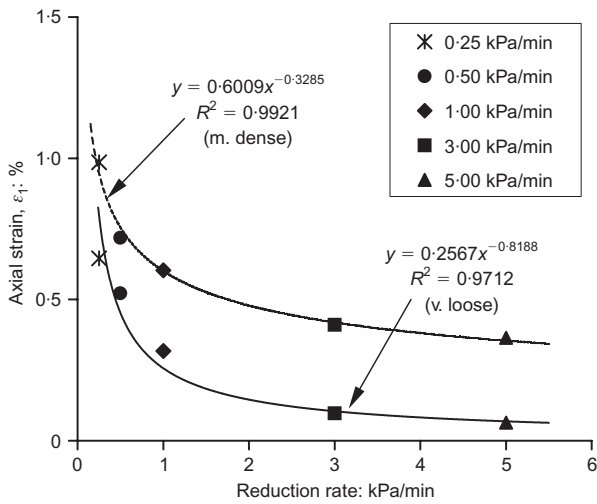


Fig. 12. Relationship between axial strain developed in CSD test and  $\sigma'_3$  reduction rate

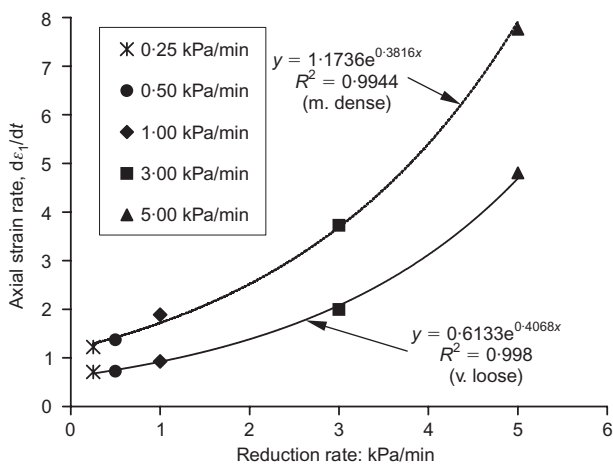


Fig. 13. Relationship between rate of axial strain developed during pre-failure instability and  $\sigma'_3$  reduction rate

The differences between the runaway and conditional instabilities are due mainly to the differences in the mean effective stress reduction mechanisms. In an undrained test the pore water pressure increases as a response to the external loading condition. Once the instability conditions are met, the pore water pressure can increase very rapidly at an accelerating rate. Thus the mean effective stress will also reduce very rapidly at an accelerating rate. However, in a drained test the reduction in the mean effective stress is controlled. There is a lack of accelerating effect. As a result, the instability is not a runaway type, although instability is developing as the strains start to develop rapidly at an accelerating rate.

It has been established by Leong (2004), Chu *et al.* (2003) and Wanatowski *et al.* (2010) that the instability conditions under both drained and undrained conditions for contractive and dilative sand can be determined by the instability line defined by Lade (1992, 1993). As the effective stress paths from either drained or undrained instability are the same, the differences that lead to conditional or runaway instability may lie in the way in which the CSD path is controlled. In an undrained instability test, the mean effective stress  $p'$  is not controlled. Its change is caused by pore pressure change. However, in a drained instability test the reduction in mean effective stress  $p'$  is automatically controlled. When the  $\sigma'_3$  reduction rate becomes equivalent

to the rate at which excess pore pressure is generated in an undrained test, the two types of instability will become similar. It is also possible that, when drained instability occurs, the amounts of axial strain and volumetric strain developed become so large that there is insufficient time for the excess pore water pressure to be dissipated fully and efficiently. Therefore the instability that has occurred initially under a drained condition may evolve into a runaway instability.

To investigate further the effect of drainage conditions on the instability of loose sand, a special plane-strain instability test IND24 was conducted (Fig. 14). This test illustrates the response of a granular soil when an undrained condition is imposed after instability is developing under drained conditions. In other words, such test simulates the condition where the amount of excess pore water pressure generated during instability under a drained loading condition becomes too large for the soil mass to dissipate efficiently.

The effective stress path and the stress-strain curve obtained from Test IND24 are presented in Figs 14(a) and 14(b) respectively. The specimen was  $K_0$ -consolidated to a mean effective stress of 200 kPa (point A in Fig. 14(a)). The void ratio of the specimen after  $K_0$ -consolidation was  $e_c = 0.903$ . From point A, the deviator load was controlled to be constant. At the same time, the back-pressure was increased at a constant rate of 0.5 kPa/min. The drainage valves were closed when point C was reached. The drained instability began to evolve at point B (Fig. 14(d)). As shown in Figs 14(a) and 14(b), the deviatoric stress reduced after point C. This was because the specimen collapsed, as indicated by the sudden increase in the excess pore water pressure and axial strain (Figs 14(c) and 14(d)), and the deviatoric stress could not be maintained by the testing machine. Photographs of the specimen at the end of Test IND24 are shown in Fig. 14(f). It was observed that after an undrained condition was imposed on the specimen, both the axial strain rate and the pore water pressure increased suddenly, and the specimen collapsed instantly. The specimen would not collapse so quickly if the drainage valves were kept open at point C. This is because at the onset of undrained instability the pore water pressure shoots up without any control, whereas the pore water pressure only increases at a constant rate during drained instability (Chu *et al.*, 2003, Wanatowski *et al.*, 2010).

Figure 14(e) shows the curve of volumetric strain against time for Test IND24. The specimen underwent volumetric dilation during the constant-load test (from point A to point B). At the onset of drained instability (point B), the specimen started to contract at a high rate. This is consistent with all the drained instability tests conducted on very loose sand. At point C an undrained condition was imposed, and the volume change of the specimen was ceased.

From the results of drained instability tests conducted with different  $\sigma'_3$  reduction rates, it can be seen that instability occurred on the same instability line, even though the  $\sigma'_3$  reduction rates were different. The reduction rate, however, affects the duration of a constant-load test under a drained condition and the amount of axial strain developed upon the instability point. It was observed that the higher the reduction rate, the less time and the less axial deformation is needed for instability to occur. The data obtained from the special instability test conducted under plane-strain conditions also imply that a conditional instability occurring under a drained condition can evolve into a runaway instability when the drainage is stopped. This means that an instability occurring under a drained condition can evolve into a runaway instability when the amount of pore water pressure generated becomes too large for the soil mass to dissipate efficiently.

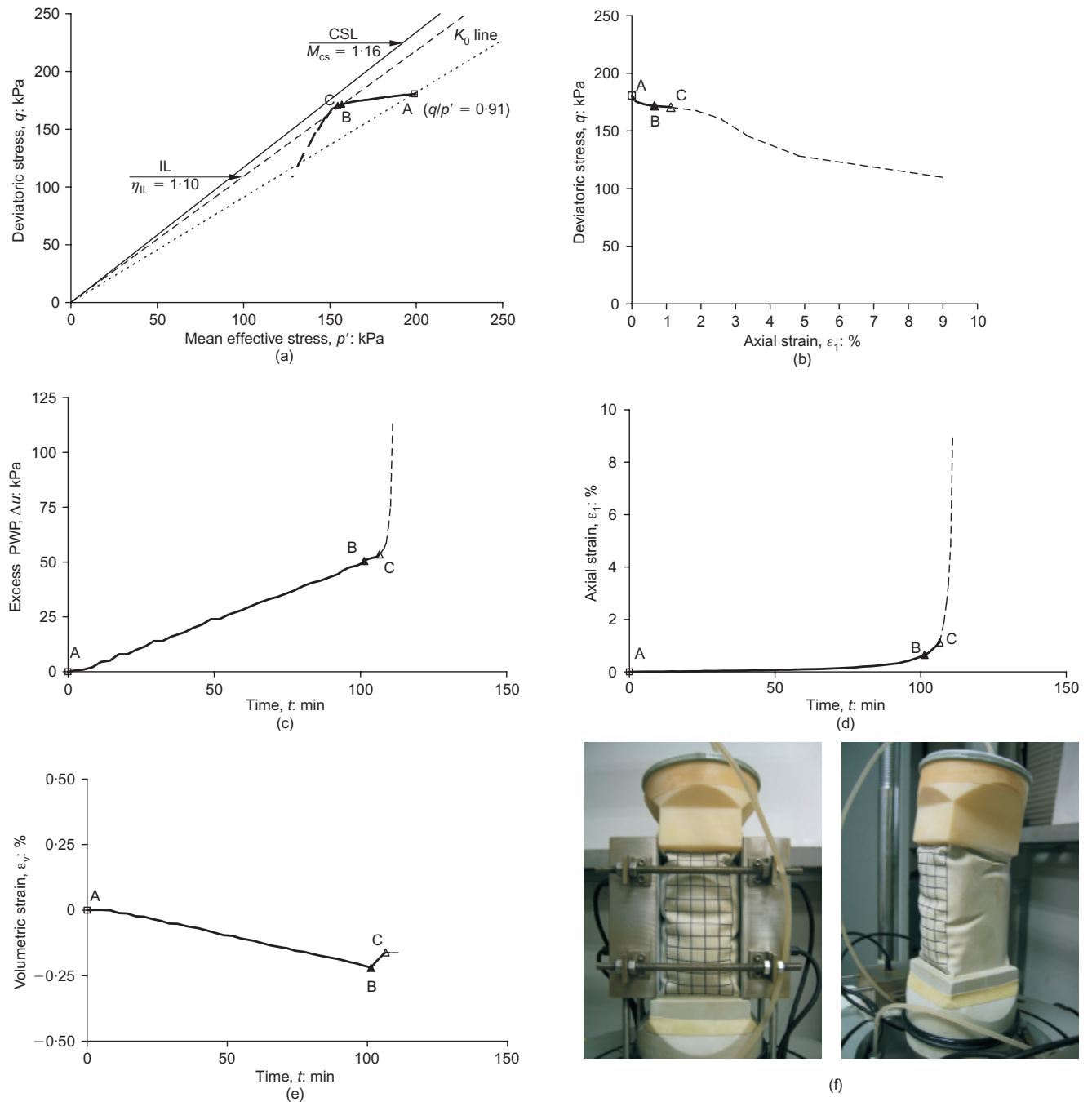


**Fig. 14. Instability behaviour of very loose sand under drained/undrained conditions (Test IND24,  $e_c = 0.903$ ): (a) effective stress path; (b) stress–strain curve; (c)  $\Delta u$  against time; (d)  $\epsilon_1$  against time; (e)  $\epsilon_v$  against time; (f) specimen at end of test (A, start of instability test; B, onset of instability; C, closure of drainage valves)**

#### Load control versus deformation control

It has been discussed by Chu & Leong (2001) and Chu & Wanatowski (2009) that the load control mode is one of the main factors affecting the occurrence of instability (or strain-softening) of soils. Although the conditions that lead to strain-softening and instability are the same, the former occurs when a specimen is sheared under a deformation-controlled loading mode and the latter under a load-controlled loading mode.

The results of a pair of  $K_0$ -consolidated tests conducted on very loose specimens under undrained conditions are presented in Fig. 15. Test U05 was conducted under a deformation-controlled (DC) loading mode and Test U05L under a load-controlled (LC) loading mode. The effective stress paths of the two tests and the CSL determined by drained tests on very loose sand (Wanatowski & Chu, 2006)

are also shown in Fig. 15(a). It can be seen that the two effective stress paths were similar, and both approached the CSL. However, the two tests ended at quite different stress points on the CSL line. This implies that the residual (or post-liquefaction) strength (Martin, 1998) obtained from the DC and LC tests will be different. In Fig. 15(a) the instability line can be drawn through the peak points of the undrained effective stress paths. Fig. 15(a) indicates that the same instability line was obtained for both the DC and the LC tests.

The stress–strain curves of the two tests are compared in Fig. 15(b). Similar pre-peak behaviour was observed in the two tests. Both peak deviatoric stresses occurred around an axial strain of 0.4%. However, the stress–strain curves in the post-peak region are different. In the DC test (U05) strain-softening behaviour was observed, whereas in the LC test

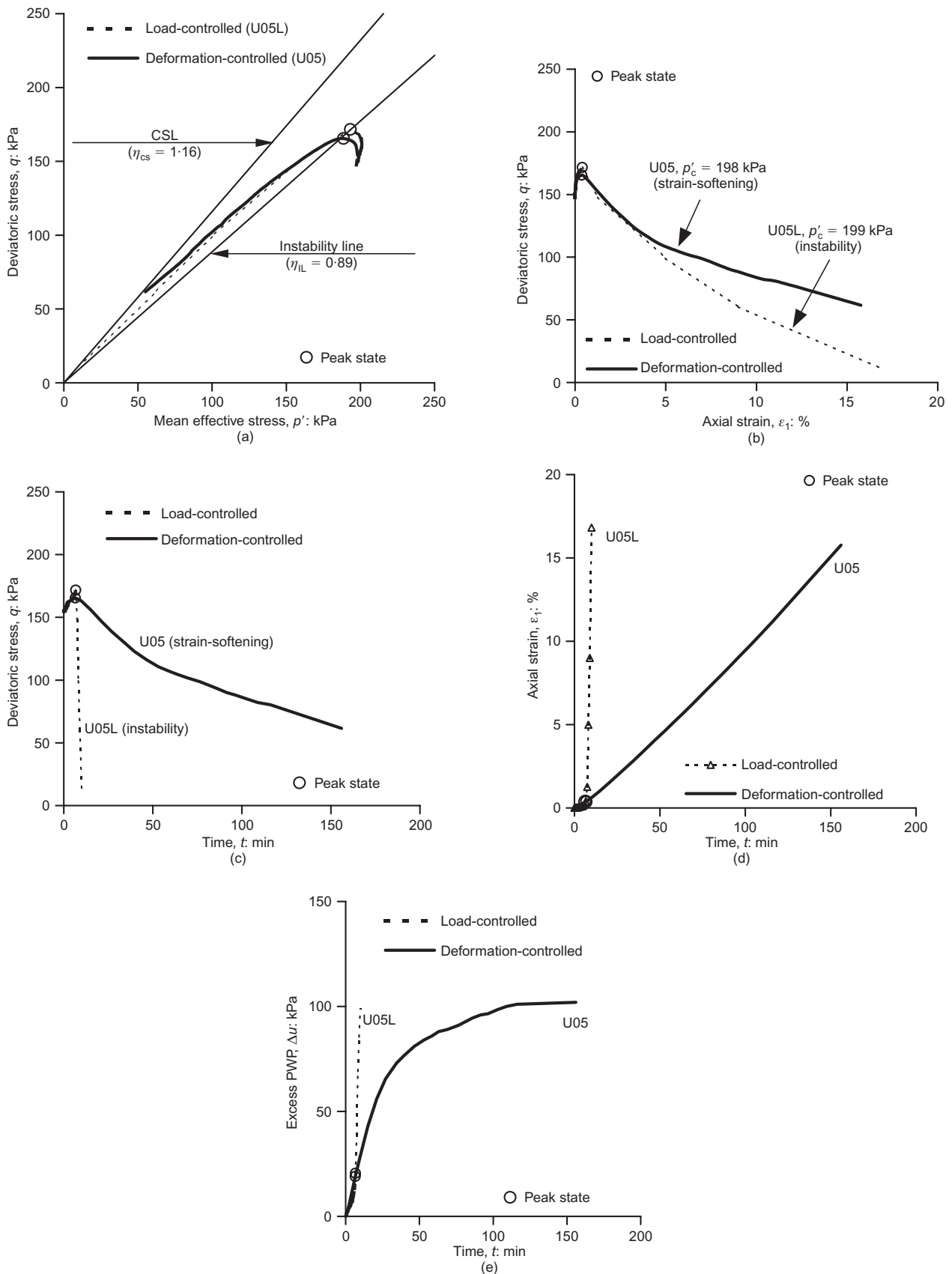


Fig. 15. Comparison of undrained tests conducted on very loose sand under deformation-controlled and load-controlled loading modes: (a) effective stress paths; (b) stress–strain curves; (c) deviatoric stress against time; (d) axial strain against time; (e) excess pore water pressure against time

(U05L) instability took place. This can be seen more clearly from Figs 15(c) and 15(d). In the LC test (U05L) the axial strain increased suddenly at the peak (Fig. 15(d)). Thus the specimen became unstable at the peak. Once the strain rate

exceeded the maximum loading rate of the force actuator, the axial load could not be maintained, and the deviatoric stress dropped suddenly at the peak (Fig. 15(c)). On the other hand, in the DC test (U05) the deviatoric stress

reduced gradually with time (Fig. 15(c)) and the axial strain increased almost linearly with time (Fig. 15(d)) in the post-peak region. Therefore strain-softening occurred in Test U05. The curves of excess pore water pressure against time are also shown in Fig. 15(e). In Test U05 the pore water pressure increased gradually, and reached a constant value at the end of shearing, whereas in Test U05L the pore water pressure shot up after the specimen became unstable at the peak (Fig. 15(e)).

From the above results it can be concluded that the post-peak stress-strain behaviour of very loose sand under undrained conditions is affected by the loading mode. Whether pre-failure instability or pre-failure strain-softening will occur in a test is affected by whether the test is conducted under a load-controlled or deformation-controlled loading mode. This observation is consistent with experimental and analytical studies carried out by Lade & Pradel (1990), Pradel & Lade (1990), di Prisco & Imposimato (1997), Chu & Leong (2001), Andrade (2009) and Daouadi *et al.* (2010).

## CONCLUSIONS

Several plane-strain tests were carried out to study the factors affecting pre-failure instability of sand under undrained and drained conditions. The following conclusions can be derived from this study.

- For loose (i.e. contractive) sand pre-failure instability occurs under both drained and undrained conditions. The conditions for the occurrence of both instabilities are the same: that is, the instability will occur when the stress state falls into the zone of instability. However, the manifestations of instability are different. The instability occurring under drained conditions is a conditional type, as it occurs only along a stress path with reduction in the mean effective stress, whereas the instability under undrained conditions is a runaway type.
- For dense (i.e. dilative) sand pre-failure instability can also occur, but only under drained conditions. Similar to drained instability of loose sand, pre-failure instability of dense sand is conditional, and occurs when the stress state of a specimen sheared along a stress path with decreasing mean effective stress crosses the instability line. However, the instability line is not unique; it varies with the void ratio of sand and applied effective stresses.
- Drained instability is different from undrained instability. The main factor that contributes to the difference is the mean effective stress reduction mechanism. In undrained tests the reduction is caused by the increase in pore water pressure, which leads to runaway instability. The strain rate developed during drained instability is dependent on the effective stress reduction rate. Therefore instability that is initiated under a drained condition may evolve into a runaway instability when drainage is impeded, or when the volume of water to be dissipated exceeds the discharge rate of the soil.
- The occurrence of pre-failure instability of sand is affected by the loading mode. Pre-failure instability will occur only when a test is conducted under a load-controlled loading mode, whereas strain-softening will take place when a test is conducted under a deformation-controlled loading mode, given the other conditions are the same.
- The results obtained from plane-strain tests have shown that the occurrence of instability under drained conditions is controlled by the sand state. This is consistent with experimental and analytical studies carried out by Chu *et al.* (2003), Been & Jefferies (2004) and Andrade (2009)

under axisymmetric conditions. However, it was found that the modified state parameter  $\bar{\psi}$ , defined as  $e_{IL} - e_{cs}$  by Chu *et al.* (2003), is more suitable for predicting the onset of instability than the state parameter  $\psi$ , defined previously as  $e_0 - e_{cs}$  by Been & Jefferies (1985). Using the modified state parameter  $\bar{\psi}$  the framework proposed by Chu *et al.* (2003) to describe the instability conditions of both contractive and dilative sand in triaxial tests can be extended into plane-strain conditions.

## NOTATION

$B$	Skempton's pore water pressure parameter
$b$	intermediate principal stress parameter
CSL	critical-state line
$CSL_{psc}$	CSL under plane-strain conditions
$CSL_{tc}$	CSL under axisymmetric conditions
$e$	void ratio
$e_0$	void ratio at initial state
$e_{cs}$	void ratio at critical state
$e_{IL}$	void ratio at instability state
IL	instability line
$K_0$	coefficient of lateral earth pressure at rest
$M_{sc}$	slope of CSL
$M_{psc}$	slope of CSL on $q-p'$ plane under plane-strain conditions
$M_{tc}$	slope of CSL on $q-p'$ plane under axisymmetric conditions
$p'$	mean effective stress
$q$	deviatoric stress
$q/p'$	effective stress ratio
$t$	time
$\Delta u$	excess pore water pressure
$\varepsilon_v$	volumetric strain
$\varepsilon_1$	axial strain
$\eta_{IL}$	gradient of instability line
$\lambda_{psc}$	slope of CSL on $e-\log p'$ plane under plane-strain conditions
$\lambda_{tc}$	slope of CSL on $e-\log p'$ plane under axisymmetric conditions
$\sigma_1, \sigma_2, \sigma_3$	major, intermediate and minor principal stresses
$(\phi_{cs})_{psc}$	critical-state friction angle under plane-strain conditions
$(\phi_{cs})_{tc}$	critical-state friction angle under axisymmetric conditions
$\psi$	modified state parameter

## REFERENCES

- Alshibli, A. K., Batiste, S. N. & Sture, S. (2003). Strain localization in sand: plane strain versus triaxial compression. *J. Geotech. Geoenviron. Engng* **129**, No. 6, 483–494.
- Anandarajah, A. (1994). Procedures for elasto-plastic liquefaction modeling of sands. *J. Engng Mech.* **120**, No. 7, 1563–1587.
- Anderson, S. A. & Riemer, M. F. (1995). Collapse of saturated soil due to reduction in confinement. *J. Geotech. Engng* **121**, No. 2, 216–220.
- Anderson, S. A. & Sitar, N. (1995). Analysis of rainfall-induced debris flows. *J. Geotech. Engng* **121**, No. 7, 544–552.
- Andrade, J. E. (2009). A predictive framework for liquefaction instability. *Géotechnique* **59**, No. 8, 673–682, <http://dx.doi.org/10.1680/geot.7.00087>.
- Been, K. & Jefferies, M. G. (1985). A state parameter for sands. *Géotechnique* **35**, No. 2, 99–112, <http://dx.doi.org/10.1680/geot.1985.35.2.99>.
- Been, K. & Jefferies, M. (2004). Stress-dilatancy in very loose sand. *Can. Geotech. J.* **41**, No. 5, 972–989.
- Been, K., Conlin, B. H., Crooks, J. H. A., Fitzpatrick, S. W., Jefferies, M. G., Rogers, B. T. & Shinde, S. (1987). Back analysis of the Nerlerk berm liquefaction slides: Discussion. *Can. Geotech. J.* **24**, No. 1, 170–179.
- Been, K., Crooks, J. H. A., Conlin, B. H. & Horsfield, D. (1988). Liquefaction of hydraulically placed sand fills. In *Hydraulic fill structures* (eds D. J. A. Van Zyl and S. G. Vick), Geotechnical Special Publication No. 21, pp. 573–591. Reston, VA: ASCE.

- Bishop, A. W. (1973). The stability of tips and spoil heaps. *Q. J. Engng Geol.* **6**, Nos 3–4, 335–376.
- Brand, E. W. (1981). Some thoughts on rain-induced slope failures. *Proc. 10th Int. Conf. Soil Mech. Found. Engng, Stockholm 3*, 373–376.
- Casagrande, A. (1965). Role of the ‘calculated risk’ in earthwork and foundation engineering. *J. Soil Mech. Found. Div. ASCE* **91**, No. SM5, 1–40.
- Casagrande, A. (1975). Liquefaction and cyclic deformation of sands: a critical review. *Proc. 5th Pan American Conf. Soil Mech. Found. Engng, Buenos Aires 5*, 79–133.
- Chu, J. & Leong, W. K. (2001). Pre-failure strain softening and pre-failure instability of sand: a comparative study. *Géotechnique* **51**, No. 4, 311–321, <http://dx.doi.org/10.1680/geot.2001.51.4.311>.
- Chu, J. & Wanatowski, D. (2008). Instability conditions of loose sand in plane-strain. *J. Geotech. Geoenviron. Engng* **134**, No. 1, 136–142.
- Chu, J. & Wanatowski, D. (2009). Effect of loading mode on strain softening and instability behavior of sand in plane-strain tests. *J. Geotech. Geoenviron. Engng* **135**, No. 1, 108–120.
- Chu, J., Lo, S.-C. R. & Lee, I. K. (1993). Instability of granular soils under strain path testing. *J. Geotech. Engng* **119**, No. 5, 874–892.
- Chu, J., Leroueil, S. & Leong, W. K. (2003). Unstable behaviour of sand and its implication for slope stability. *Can. Geotech. J.* **40**, No. 5, 873–885.
- Cornforth, D. H. (1964). Some experiments on the influence of strain conditions on the strength of sand. *Géotechnique* **14**, No. 2, 143–167, <http://dx.doi.org/10.1680/geot.1964.14.2.143>.
- Daouadji, A., AlGali, H., Darve, F. & Zeghloul, A. (2010). Instability of granular materials: experimental evidence of diffuse mode of failure for loose sands. *J. Engng Mech.* **136**, No. 5, 575–588.
- Desrues, J. & Viggiani, G. (2004). Strain localization in sand: an overview of the experimental results obtained in Grenoble using stereophotogrammetry. *Int. J. Numer. Analyt. Methods Geomech.* **28**, No. 4, 279–321.
- di Prisco, C. & Imposimato, S. (1997). Experimental analysis and theoretical interpretation of triaxial load controlled loose sand specimen collapses. *Mech. Cohesive-Frict. Mater.* **2**, No. 2, 93–120.
- Eckersley, J. D. (1990). Instrumented laboratory flowslides. *Géotechnique* **40**, No. 3, 489–502, <http://dx.doi.org/10.1680/geot.1990.40.3.489>.
- Finno, R. J., Harris, W. W. & Viggiani, G. (1996). Strain localization and undrained steady state of sand. *J. Geotech. Engng* **122**, No. 6, 462–473.
- Finno, R. J., Harris, W. W., Mooney, M. A. & Viggiani, G. (1997). Shear bands in plane strain compression of loose sand. *Géotechnique* **47**, No. 1, 149–165, <http://dx.doi.org/10.1680/geot.1997.47.1.149>.
- Fleming, R. W., Ellen, S. D. & Albus, M. A. (1989). Transformation of dilative and contractive landslide debris into debris flows: an example from Marin County, California. *Engng Geol.* **27**, Nos 1–4, 201–223.
- Han, C. & Vardoulakis, I. G. (1991). Plane-strain compression experiments on water-saturated fine-grained sand. *Géotechnique* **41**, No. 1, 49–78, <http://dx.doi.org/10.1680/geot.1991.41.1.49>.
- Imam, S. M. R., Morgenstern, N. R., Robertson, P. K. & Chan, D. H. (2002). Yielding and flow liquefaction of loose sand. *Soils Found.* **42**, No. 3, 19–31.
- Jefferies, M. G. & Shuttle, D. A. (2002). Dilatancy in general Cambridge-type model. *Géotechnique* **52**, No. 9, 625–638, <http://dx.doi.org/10.1680/geot.2002.52.9.625>.
- Lade, P. V. (1992). Static instability and liquefaction of loose fine sandy slopes. *J. Geotech. Engng* **118**, No. 1, 51–71.
- Lade, P. V. (1993). Initiation of static instability in the submarine Nerlerk berm. *Can. Geotech. J.* **30**, No. 6, 895–904.
- Lade, P. V. & Pradel, D. (1990). Instability and plastic flow of soils. I: Experimental observations. *J. Engng Mech.* **116**, No. 11, 2532–2550.
- Lade, P. V., Nelson, R. B. & Ito, Y. M. (1987). Nonassociated flow and stability of granular materials. *J. Engng Mech.* **113**, No. 9, 1302–1318.
- Lade, P. V., Yamamuro, J. A. & Bopp, P. A. (1997). Influence of time effects on instability of granular materials. *Comput. Geotech.* **20**, No. 3–4, 179–193.
- Leong, W. K. (2004). *Instability behaviour of granular fill material*. PhD thesis, Nanyang Technological University, Singapore.
- Leong, W. K. & Chu, J. (2002). Effect of undrained creep on instability behaviour of loose sand. *Can. Geotech. J.* **39**, No. 6, 1399–1405.
- Leong, W. K., Chu, J. & Teh, C. I. (2000). Liquefaction and instability of a granular fill material. *Geotech. Test. J. ASTM* **23**, No. 2, 178–192.
- Lo, S.-C. R. & Chu, J. (1991). The measurement of  $K_0$  by triaxial strain path testing. *Soils Found.* **31**, No. 2, 181–187.
- Lo, S.-C. R., Chu, J. & Lee, I. K. (1989). A technique for reducing membrane penetration and bedding errors. *Geotech. Test. J., ASTM* **12**, No. 4, 311–316.
- Loke, W. L. (2004). *Failure mechanisms of gentle granular slopes*. MEng thesis, Nanyang Technological University, Singapore.
- Martin, G. R. (1998). Post-liquefaction shear strength from laboratory and field tests. *Proceedings of the National Science Foundation workshop on shear strength of liquefied soils*, Urbana, IL, pp. 40–52.
- Mokni, M. & Desrues, J. (1998). Strain localisation measurements in undrained plane-strain biaxial tests on Hostun RF sand. *Mech. Cohes.-Frict. Mater.* **4**, No. 4, 419–441.
- Mroz, Z., Boukpeti, N. & Drescher, A. (2003). Constitutive model for static liquefaction. *Int. J. Geomech.* **3**, No. 3, 133–144.
- Olson, S. M., Stark, T. D., Walton, W. H. & Castro, G. (2000). 1907 static liquefaction flow failure of the north dike of Wachusest dam. *J. Geotech. Geoenviron. Engng* **126**, No. 12, 1184–1193.
- Orense, R., Farooq, K. & Towhata, I. (2004). Deformation behaviour of sandy slopes during rainwater infiltration. *Soils Found.* **44**, No. 2, 15–30.
- Pradel, D. & Lade, P. V. (1990). Instability and plastic flow of soils. II: Analytical investigation. *J. Engng Mech.* **116**, No. 11, 2551–2566.
- Rowe, P. W. & Barden, L. (1964). Importance of free ends in triaxial testing. *J. Soil Mech. Found. Div. ASCE* **90**, No. SM1, 1–15.
- Sasitharan, S., Robertson, P. K., Segoo, D. C. & Morgenstern, N. R. (1993). Collapse behaviour of sand. *Can. Geotech. J.* **30**, No. 4, 569–577.
- Sento, N., Kazama, M., Uzuoka, R., Ohmura, H. & Ishimaru, M. (2004). Possibility of postliquefaction flow failure due to seepage. *J. Geotech. Geoenviron. Engng* **129**, No. 8, 727–737.
- Skopek, P., Morgenstern, N. R., Robertson, P. K. & Segoo, D. C. (1994). Collapse of dry sand. *Can. Geotech. J.* **31**, No. 6, 1008–1014.
- Sladen, J. A., D’Hollander, R. D., Krahn, J. & Mitchell, D. E. (1985). Back analysis of the Nerlerk berm liquefaction slides. *Can. Geotech. J.* **22**, No. 4, 579–588.
- Torrey, V. H. & Weaver, F. J. (1984). Flow failures in Mississippi riverbanks. *Proc. 4th Int. Symp. on Landslides, Toronto 2*, 335–360.
- Verdugo, R. & Ishihara, K. (1996). The steady state of sandy soils. *Soils Found.* **36**, No. 2, 81–91.
- Wanatowski, D. (2005). *Strain softening and instability of sand under plane-strain conditions*. PhD thesis, Nanyang Technological University, Singapore.
- Wanatowski, D. & Chu, J. (2006). Stress–strain behavior of a granular fill measured by a new plane-strain apparatus. *Geotech. Test. J. ASTM* **29**, No. 2, 149–157.
- Wanatowski, D. & Chu, J. (2007). Static liquefaction of sand in plane-strain. *Can. Geotech. J.* **44**, No. 3, 299–313.
- Wanatowski, D., Chu, J. & Loke, W. L. (2010). Drained instability of sand in plane-strain. *Can. Geotech. J.* **47**, No. 4, 400–412.
- Wang, Z.-L., Dafalias, Y. F., Li, X.-S. & Makdisi, F. I. (2002). State pressure index for modeling sand behavior. *J. Geotech. Geoenviron. Engng* **128**, No. 6, 511–519.
- Yang, J. (2002). Non-uniqueness of flow liquefaction line for loose sand. *Géotechnique* **52**, No. 10, 757–760, <http://dx.doi.org/10.1680/geot.2002.52.10.757>.